Fracture analysis approach of DP600 steel when subjected to different stress/strain states during deformation

Luiz Mauricio Valente Tigrinho, Ravilson Antonio Chemin Filho & Paulo Victor Prestes Marcondes

The International Journal of Advanced Manufacturing Technology

ISSN 0268-3768

Int J Adv Manuf Technol
DOI 10.1007/s00170-013-5104-9

Springer

Int J Adv Manuf Technol
DOI 10.1007/s00170-013-5104-9

ORIGINAL ARTICLE

Fracture analysis approach of DP600 steel when subjected to different stress/strain states during deformation

Luiz Mauricio Valente Tigrinho · Ravilson Antonio Chemin Filho · Paulo Victor Prestes Marcondes

Received: 11 July 2012 / Accepted: 28 May 2013

Abstract One of the major manufacturing processes to produce components from flat sheets is forming. The automotive industry is one of the highest markets for stamped parts and is, thus, a major driving force for the development of new materials and technologies. In recent decades, there is increasing competition and growing demand for light weight, high-performance, and crashworthiness structures in the automotive vehicle forced steel industry, automakers, and the scientific community to focus more on efficient manufacturing. In recent decades, the increasing competition and growing demand for steel structures in automobiles was observed, especially for advanced high-strength steel (AHSS) parts. Thus, a better understanding of the formability of these materials is necessary to reduce costs and optimize the process. In order to better understand the mechanical behavior of AHSS, many authors have been researching the fracture aspects related to the stamping conditions. The main aim of this study was to analyze the type of fracture in DP600 steel when subjected to different stress/strain states (uniaxial and biaxial stress and plane strain) imposed by deep drawing and stretching. The experimentations led to a detailed understanding of the influence of stress/strain state in the mechanism of fracture, particularly, under plane strain—which showed quasi-cleavage regions surrounded by dimples. In addition, the microstructural analysis confirmed that the DP600 steel can show ductile fractures with some aspects of brittle behavior, depending of which stress/strain state was used for deformation. As a result, the DP600 forming limit curve related to micromechanisms of fracture generated by uniaxial and biaxial tensile stress and plane strain was presented.

Keywords DP600 formability · Stress/strain states influence · Ductile/brittle fracture

1 Introduction

Aimed efficiency in the manufacture and definition of material formability and process parameter values are critical to the process. The trial-and-error procedure during forming often results in change in design of the tool to safely stamp the product. These changes in design could occur due to the use of a new material with better formability, adjustments to the design of tools, and/or variation in process parameters. Thus, in order to avoid the trial-and-error procedure, it is necessary to understand the formability of these materials in a better way for cost reduction and process optimization.

Formability evaluation is complex due to several process parameters that individually or in combination plays an influential role in the sheet metal stamping process. Researchers are continuously trying to understand the advantages and limitations of these parameters and, particularly, the influence on fracture behavior in the use of advanced high-strength steels (AHSS).

Anderson [1] reported that all ductile fracture occurs by dimple rupture mechanisms. Already, the mechanism of fracture by cleavage absorbs little energy and the fracture by this mechanism is always fragile. The intergranular (decohesive rupture) mechanism in metals is considered abnormal, i.e., its occurrence is an indication that some mechanism of embrittlement occurred during the production or use of the material, while the striations rupture mechanism is characteristic when the fracture occurs by fatigue.

Wulpi [2] also proposed a classification for the different modes of fractures that occurs in metals. He reported that the

L. M. Valente Tigrinho
Departamento de Mecânica, Instituto Federal do Paraná,
Av. Salgado Filho, 1474, CEP 81510-000 Curitiba, Paraná, Brazil

R. A. Chemin Filho · P. V. Prestes Marcondes (✉)
DEMEC, Universidade Federal do Paraná,
Av. Cel. Francisco H. dos Santos, 210, Caixa Postal 19011,
CEP 81531-990 Curitiba, Paraná, Brazil
e-mail: marcondes@ufpr.br

Published online: 09 June 2013

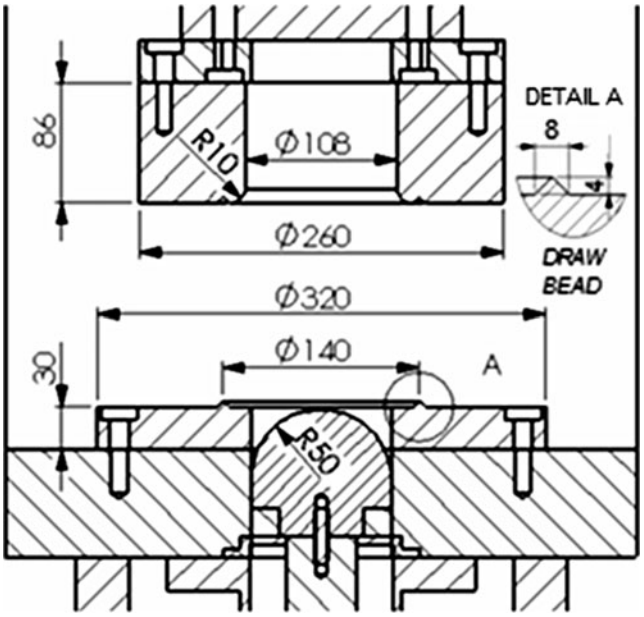

Fig. 1 Hemispherical punch with a radius of 50 mm with drawbeads in the blankholder (dimensions in millimeters)

metal may fracture by shearing or cleavage. The failure will depend on how the crystal structure of the material behaves under a given load. According to the author, the fracture by shear is primarily ductile and the onset is the dimple rupture mechanism, while the cleavage is seen as a cracking of the hard grains, i.e., a brittle fracture. The intergranular fracture is fragile and is specifically caused by a process of weakening of grain boundaries, which become weaker in relation to the interior of the grains. In this case, the fracture occurs preferentially along the grain boundaries and not through them.

The essential difference between a ductile and a brittle fracture is the mechanism of propagation that in the first case is stable—occurs under increasing load—and in the second case is unstable—occurs when a certain critical stress is reached [3]. In recent years, several studies have investigated the micromechanics of the fracture of AHSS.

Narayanasamy et al. [4, 5] reported studies in the fracture of high-strength low-alloy (HSLA), microalloyed and carbon–manganese steels under three different stress/strain states, namely, tensile–compressive stress, biaxial tensile stress, and plane strain. The analyses by scanning electron microscope (SEM) found ductile fracture with some peculiarities in the dimples. They reported elongated dimples—mainly in HSLA—due to the presence of second phase particles. In microalloyed and carbon–manganese steels, they also observed elongated dimples, but the presence of equiaxed or hemispheroidal dimples was dominant. Another important observation was the formation of voids around second phase particles.

Huh et al. [6] carried out tests by varying the strain rate from 0.003 to 200 s^{-1} using transformation induced by plasticity (TRIP) and dual-phase (DP) steels. In their work, TRIP600, TRIP800, DP600, and DP800 steels were characterized by uniaxial tensile tests. The experiments pointed out that, for all cases, the fracture showed ductile behavior. The difference reported was that, with high strain rates, the morphology of the dimples appeared higher and deeper, affecting the ductility of the material.

Kadkhodapour et al. [7] performed uniaxial tensile tests using DP800. The tests were interrupted at several stages before the rupture of the sample. They observed that some fractures were nucleated in ferrite–ferrite grain boundaries and occurred in the vicinity of martensite particles. In the ferrite–martensite grain boundaries, two onsets of crack patterns were observed. In the first pattern, a crack formed initially in the grain boundaries of ferrite–ferrite spreads to meet the grain boundary of ferrite–martensite. The second pattern was named normal separation of the ferrite–martensite grain boundaries and the crack pattern was credited to the

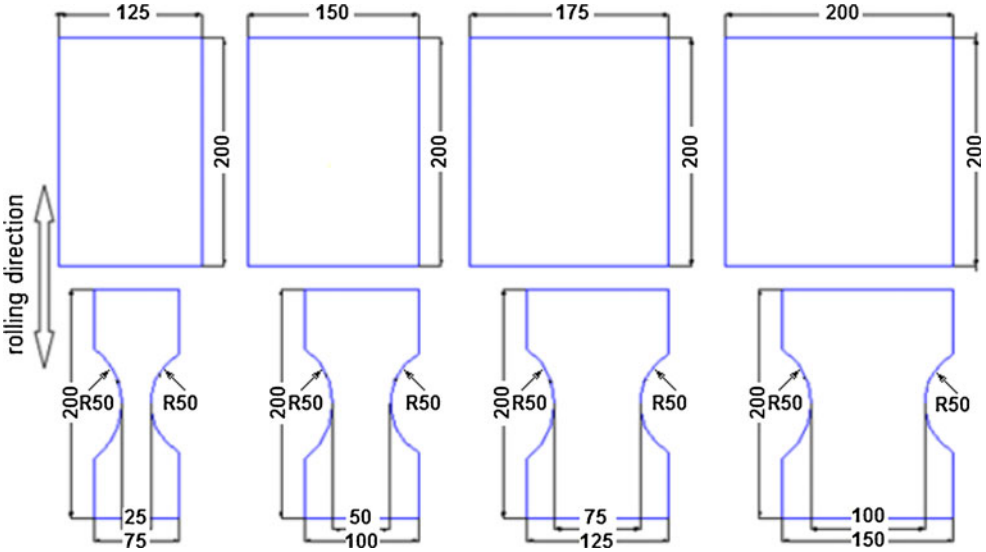

Fig. 2 Test specimens used to evaluate the FLC and the micromechanisms of fracture generated by uniaxial and biaxial tensile stress and plane strain

Table 1 DP600 chemical composition (wt %)

DP600 chemical composition (wt%)									
C	Si	Mn	P	S	Al	Cr	Mo	Nb	Ti
0.086	0.053	1.739	0.027	0.007	0.031	0.048	0.226	0.028	0.004

incompatibility of stress/strain concentration. Thus, the failure pattern was not deviated from the classical ductile fracture.

Cingara et al. [8] reported an analysis of the effect of the morphology and distribution of martensite on the mechanical properties of DP600 steels. The steels used by the author showed a martensite volume fraction of approximately 20 %, but with different chemical compositions. By SEM investigation, the author stated that the nucleation of dimples occurred in three ways: cracking of martensite, separation in regions adjacent to the martensite interface, and discontinuity in the interface of ferrite–martensite. Thus, Cingara et al. [8] concluded that a more uniform distribution of martensite in the steel led to a lower rate of growth of dimples and a continuous nucleation of this voids during the deformation process—resulting in a high density of voids before fracture. The steels that showed a higher concentration of martensite in some regions experienced an accelerated growth of voids in the thickness direction of the sheet and a catastrophic coalescence in the transverse direction of the applied load. As a result, the steels showed a commitment of the mechanical properties.

Kim et al. [9] reported an analysis of the mechanical properties and drawability of low-carbon steel and DP steel (DP590) formed with low strain rates (from 0.001 to 0.01 s^{-1}) and high strain rates (from 0.1 to 100 s^{-1}). Under these conditions, an observation on the increase of some points of cleavage among the dimples with high strain rate was made—especially for the DP590 steel. With the increase of the speed of strain, the material tends toward a condition, at least initially, of brittle fracture under biaxial tensile state. According to the authors, the forming limit curve (FLC) falls under biaxial stress state—when deformed at high speeds. This phenomenon was explained due the occurrence of shear fractures which implies a reduction of ductility of the material.

Kim et al. [10] conducted a study of AHSS failure behavior, trying to describe the onset of shear fracture. They carried out experimental and numerical studies, using DP590, DP780, and DP980 steels, and tried to accurately predict the onset of crack. In their work, they proposed a bending model for the prediction of failure—by numerical simulation—using a thermomechanical approach. According to Kim et al. [10], the crack produced after bending corresponds to a shear fracture and it is due to localized necking caused by the tensile stresses during bending. There is also the possibility that this type of fracture occurs due to the stress/strain state imposed that can promote a weakening of the material during bending.

The analysis of the failure behavior during the stamping of AHSS became, therefore, essential to manufacture efficiency. In order to advance the subject a little further and as a contribution to the research gap still present in the state of the art, the current work aimed to analyze the fracture behavior of DP600 steel sheets. In order to do so, the next sections will study the influence of the stress/strain states on the fracture of DP600 steel, i.e., under uniaxial and biaxial tensile stress and plane strain. As a contribution, a DP600 FLC related to micromechanisms of fracture generated by uniaxial and biaxial tensile stress and plane strain was proposed.

2 Experimental procedure

The sheet material used was 2-mm thick, high-strength AHSS DP600 steel. The uniaxial tensile tests were performed according to NBR 6673 [11] and NBR 8164 [12] standards and five specimens for each sheet rolling direction were used.

The tests to determine the FLC were performed according to the model originally proposed by Keeler [13] and extended by Narayanasamy et al. [4, 5, 14] and Sahu et al. [15]. The tests were conducted with a hemispherical punch with a radius of 50 mm and drawbeads in the blankholder, as described by Nakazima [16], shown in Fig. 1. The blankholder force of 130-tons and punch velocity of 10^{-3} m/s were used. Three specimens with a length of 200 mm and widths of 200, 175, 150, 125, 100, 75, 50, and 25 mm were used to create the FLC—same dimensions and quantities used by Sahu et al. [15]. No lubrication was added to the tooling or specimens. The obtained FLC curve was used as the base for generating the DP600 FLC related to micromechanisms of fracture generated by uniaxial and biaxial tensile stress and plane strain states (Fig. 10).

A 4.2-mm-diameter circle grid was imprinted on the test specimen's surface. The grid was plotted using the electrolytic process. Figure 2 illustrates the test specimens used to evaluate the FLC and the measured points of true strains. The measurements were taken on the opposite side of the fracture; therefore,

Table 2 DP600 mechanical properties

DP600 mechanical properties			
Properties	YS (MPa)	UTS (MPa)	El (%)
Standard EN 10338	340–420	≥600	≥20
Uniaxial tensile test	385	602	23.0

Table 3 DP600 drawability parameters

DP600 drawability parameters									
Parameter	$\overline{R}$	$R_{0°}$	$R_{45°}$	$R_{90°}$	ΔR	n_{average}	$n_{0°}$	$n_{45°}$	$n_{90°}$
Uniaxial tensile test	0.94	0.68	1.04	1.00	0.20	0.19	0.19	0.19	0.18

the measurements in cracked circles were avoided. The printed circles were measured with a calibrated transparent Mylar tape with diverging traces (the method was previously calibrated at an optical profilometer). An average of three test specimens for each one of the experimental conditions was evaluated.

Finally, in order to analyze the fracture of the DP600 steel submitted to different stress/strain states (uniaxial and biaxial tensile stress and plane strain), images in an SEM were taken. SEM fractographs with magnifications of ×750 and ×2,500 of the fractured region of each sample were analyzed.

3 Results

The DP600 chemical composition, mechanical properties, and drawability parameters are shown in Tables 1, 2, and 3. Figure 3 illustrates the DP600 uniaxial tensile curve. Figure 4 shows the SEM images of the DP600 steel which illustrates regions of hard phase (martensite) dispersed in a soft matrix (ferrite).

Through image analysis, the amount of each phase present in the material was determined. Ferrite in the volume fraction of 83.5 % was found, while the fraction of martensite was 16.5 %. Bucher and Hamburg [17] reported 15 % and DeArdo reported [18] 19 % of martensite in the microstructure for similar steel. Uthaisangsuk et al. [19] reported that a larger island of martensite dispersed in the ferritic matrix reduces the elongation to fracture of the DP600 steel. On the other hand, if the martensite is in the form of fine fibrous or fine globules along the contours of the ferrite, as shown in Fig. 4b, the material can show a tendency of larger elongation to fracture. Figures 5 and 6 illustrate the DP600 FLC and the test specimens used to analyze the fracture.

In this work, specimens with dimensions of 25×200, 50×200, 75×200, 100×200, and 125×200 mm represent the strain paths varying from uniaxial to plane strain conditions, whereas specimens with dimensions of 150×200, 175×200, and 200×200 mm represent the strain paths varying from biaxial to plane strain conditions—similar to those presented by Sahu et al. [15]. Figures 7, 8, and 9 show the DP600 SEM fractographs for uniaxial and biaxial tensile stress and plane strain states.

After the SEM analysis of fractures generated by the different states of stress and strain, the DP600 FLC was improved by adding the micromechanisms of fracture observed for each state (Fig. 10).

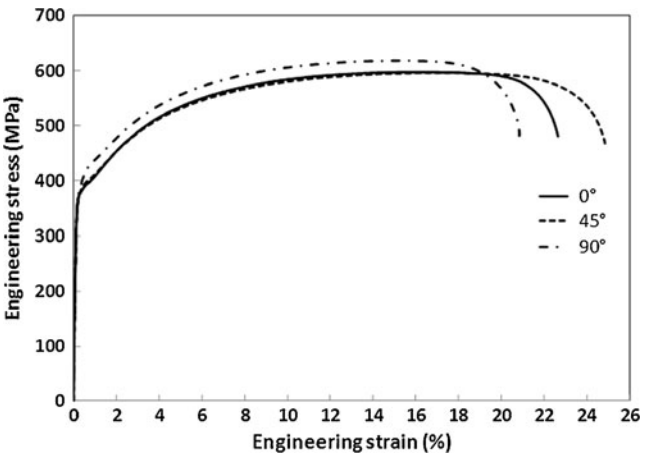

Fig. 3 DP600 uniaxial tensile curve

4 Discussion

The analysis by SEM fractographs showed that the rolling direction did not present significant influence on the fracture behavior of steel DP600 (0°, 45°, and 90°). In all cases, only

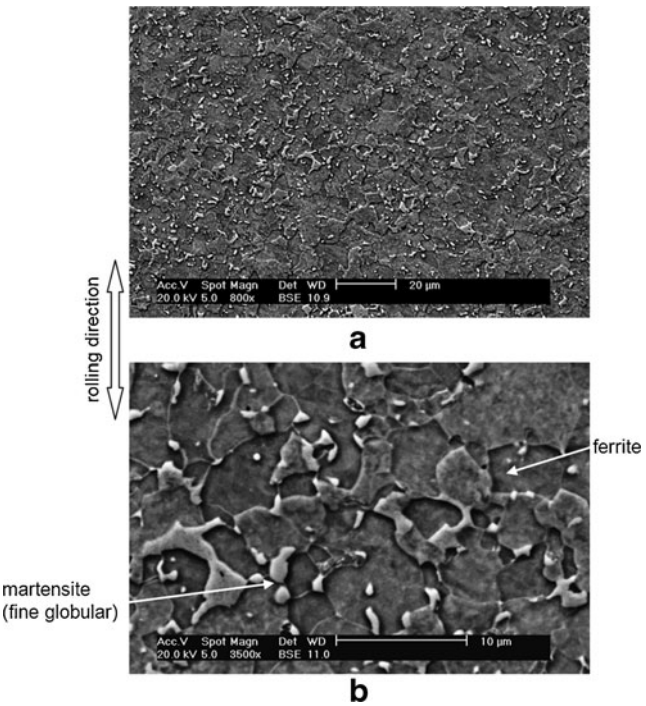

Fig. 4 DP600 SEM micrograph—martensite islands in a ferritic matrix: **a** ×800 and **b** ×3,500

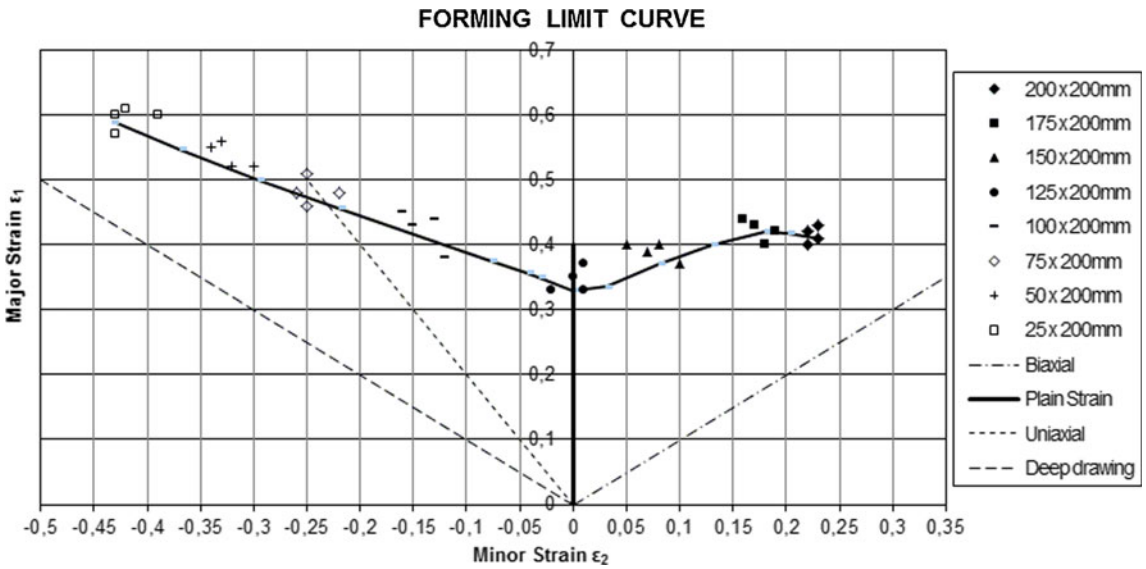

Fig. 5 DP600 FLC obtained with BHF of 130 tons and punch velocity of 10^{-3} m/s

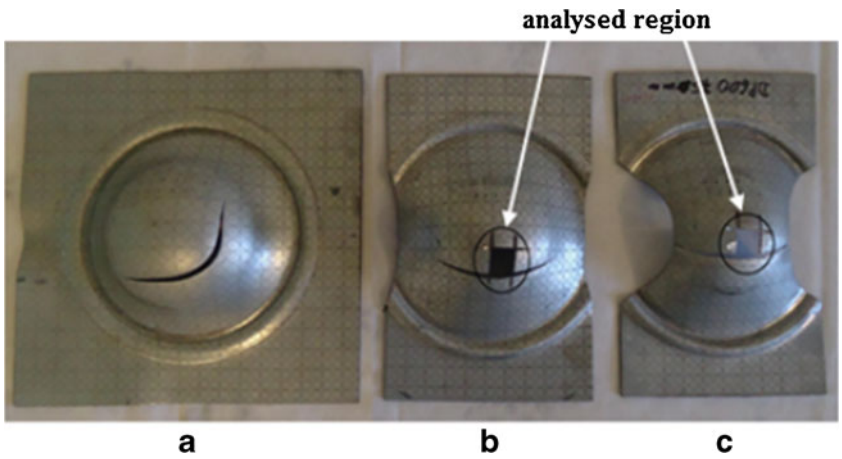

Fig. 6 Specimens for the different stress/strain states: **a** CP 200×200 mm—biaxial tensile stress, **b** CP 125×200 mm—plane strain, and **c** CP 75×200 mm—uniaxial tensile stress

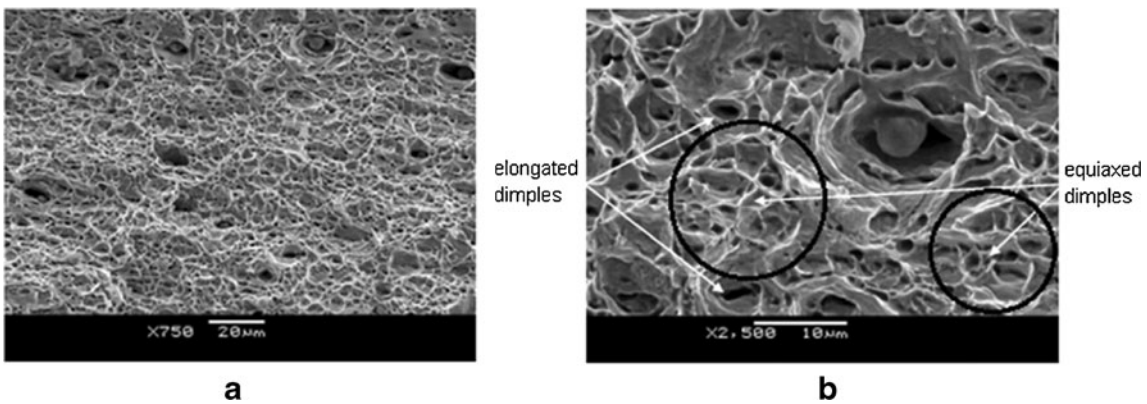

Fig. 7 DP600 SEM fractographs for uniaxial stress state—specimen 75×200 mm: **a** ×750 and **b** ×2,500

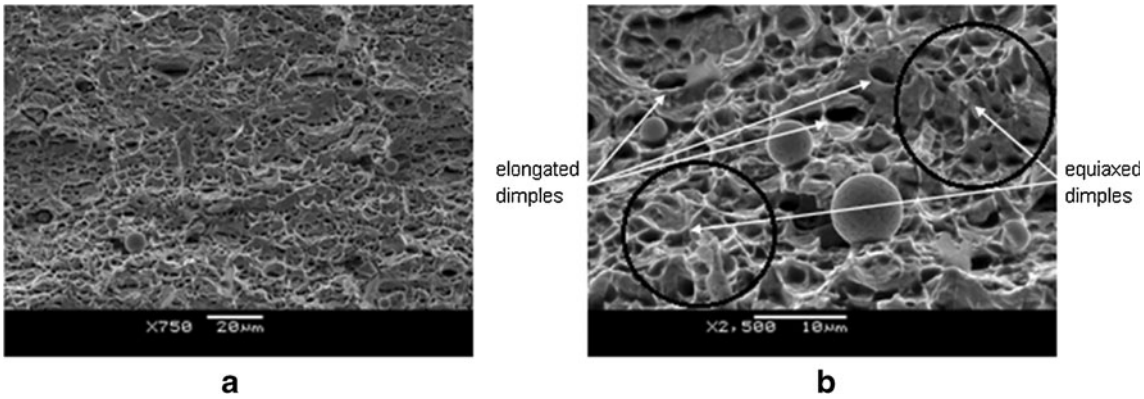

Fig. 8 DP600 SEM fractographs for biaxial stress state—specimen 200×200 mm: **a** ×750 and **b** ×2,500

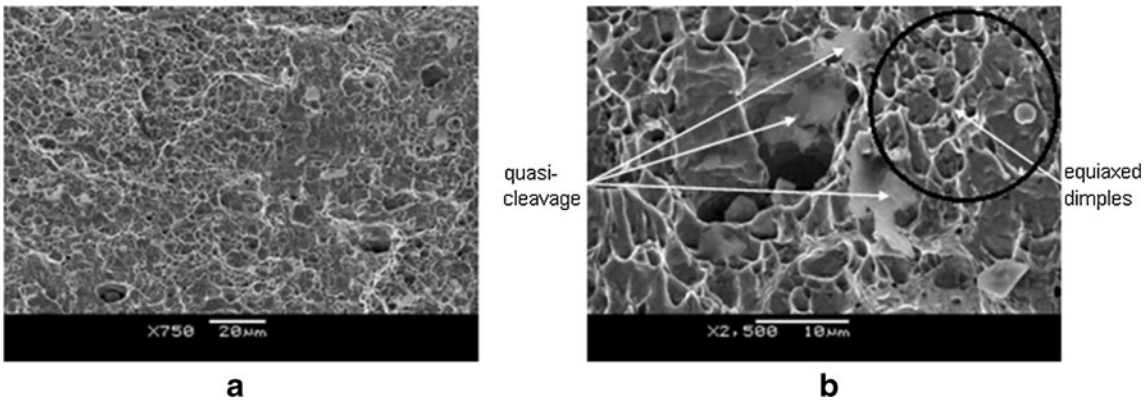

Fig. 9 DP600 SEM fractographs for plane strain state—specimen 125×200 mm: **a** ×750 and **b** ×2,500

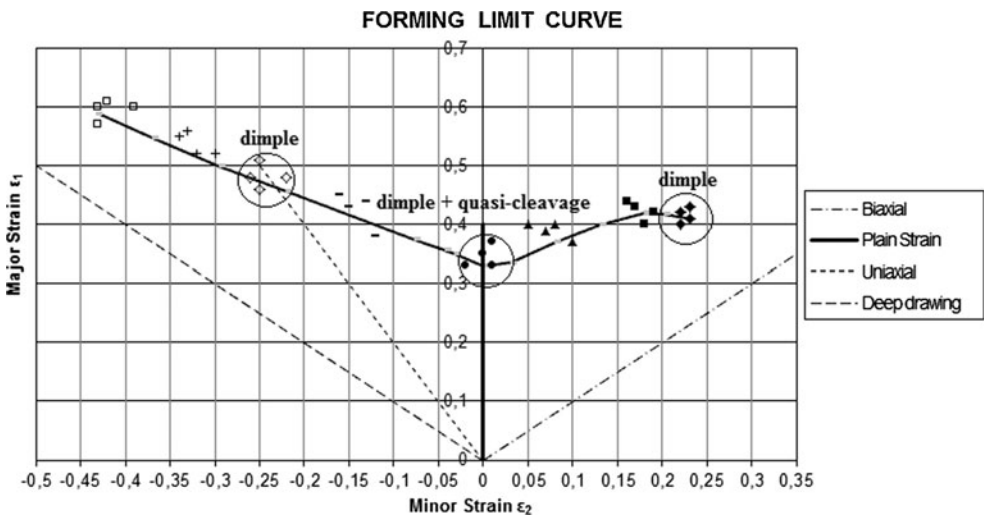

Fig. 10 Proposed DP600 FLC related to the micromechanisms of fracture generated by uniaxial and biaxial tensile stress and plane strain states

ductile fracture was observed—formed by dimples homogeneously distributed with certain amounts of rounded particles inside (Fig. 7). It is worth noting that the material shows, predominantly, not only equiaxed or hemispheroidal dimples but some elongated dimples also appeared. This finding could be explained because the fracture occurred precisely in the sheet rolling direction, which presents an alignment of the grains due to the manufacturing process. Figure 8, for the biaxial stress state, also shows predominance of equiaxed or hemispheroidal dimples, but with larger amount of elongated dimples.

Figure 9, for the plane strain state, illustrates that, despite the predominance of ductile fracture (dimples), the material showed regions with characteristics of fragile fracture (quasi-cleavage). The hypothesis presented was that the fracture happened exactly in the region of the sheet in contact with the punch radius—tensile tear—leading to fracture with brittle aspects. This fact is corroborated by the presence of a certain amount of martensite cracking, i.e., quasi-cleavage.

For other cases—with the uniaxial and biaxial tensile states—the assumption is that only ductile fractures could occur (with the presence of equiaxed or hemispheroidal dimples) because the rolling direction effect was not sufficient to change the condition of ductile failure (even with the material presenting a certain amount of hard phase). This condition could be changed with a greater presence of the hard phase of martensite on the microstructural level, i.e., as present in DP800 and DP1000 steels, or even another AHSS, such as TRIP and complex phase (CP) steels.

Several theoretical and numerical models have been and are being developed to calculate or predict the onset and propagation of fracture. An example is the approach of Gurson–Tvergaard–Needleman used for ductile fracture analysis. With the utilization of this approach, Ramazini et al. [20] reported the ductile fracture of the DP600 steel under the stamping process. Lian et al. [21] also carried out stamping studies for the DP600 steel using the numerical model. It has been reported that, despite the fact that the numerical simulation can help the research, a frequent problem of these models is the determination of its parameters, which are usually identified using experimental methods of trial-and-error procedures. In this experimental work, a summary of the micromechanisms of fracture through the FLC is shown in Fig. 10, showing that the fracture of DP600 steel shows predominantly ductile fracture regions (under states of uniaxial and biaxial stresses), but was also present in regions of ductile fracture combined to brittle fracture (in plane strain state). This important finding probably could not be identified by theoretical or numerical models.

5 Conclusion

In practical terms, when the DP600 steel was deformed in the uniaxial and biaxial tensile stresses, mostly ductile fractures (dimples) were found. In contrast, under the plane strain state, the material showed a combined mode of failure. In other words, the material presented points of brittle fracture—represented by the mechanism of quasi-cleavage or hard phase cracking—but the failure was still predominantly ductile (since dimples were still predominantly observed). To resume, it is worth reporting that DP600 shows ductile fracture with some aspects of brittle behavior, depending on which stress/strain state was used for deformation. Thus, the proposed DP600 FLC related to the micromechanisms of fracture generated by uniaxial and biaxial tensile stress and plane strain states can help us better understand the conformability of this material.

Acknowledgments The authors thank the financial support from CNPq Agency for the scholarship and the steel samples supplied by Usinas Siderúrgicas de Minas Gerais S/A (USIMINAS).

References

1. Anderson TL (1995) Fracture mechanics—fundamentals and applications, 2nd edn. CRC, Boca Raton
2. Wulpi DJ (1999) Understanding how components fail, 2nd edn. ASM International, Novelty
3. ASM International (1993) Metals handbook, vols. 12 and 14, 9th edn. ASM International, Materials Park
4. Narayanasamy R, Parthasarathi NL, Sathiiya Narayanan C, Venugopal T, Pradhan HT (2008) A study on fracture behaviour of three different high strength low alloy steel sheets during formation with different strain ratios. Mater Des 29:1868–1885
5. Narayanasamy R, Parthasarathi NL, Sathiya Narayanan C (2009) Effect of microstructure on void nucleation and coalescence during forming of three different HSLA steel sheets under different stress. Mater Des 30:1310–1324
6. Huh H, Kim SB, Song JH, Lim JH (2008) Dynamic tensile characteristics of TRIP-type and DP-type steel sheets for an auto-body. Int J Mech Sci 50:918–931
7. Kadkhodapour J, Butz A, Ziaei-Rad, Schmauder S (2011) A micro mechanical study on failure initiation of dual phase steels under tension using single crystal plasticity model. Int J Plast 27:1103–1125
8. Cingara GA, Ososkov Y, Jain MK, Wilkinson DS (2009) Effect of martensite distribution on damage behaviour in DP600 dual phase steels. Mater Sci Eng, A 516:7–16
9. Kim SB, Huh H, Bok HH, Moon MB (2011) Forming limit diagram of auto-body steel sheets high-speed sheet metal forming. J Mater Process Technol 211:851–862
10. Kim RJ, Sung JH, Piao K, Wagoner RH (2011) The shear fracture of dual-phase steel. Int J Plast 27:1658–1676
11. Brazilian Technical Standards Association, NBR 6673 (1981) Produtos Planos de Aço—Determinação das Propriedades Mecânicas a Tração, Brazil
12. Brazilian Technical Standards Association, NBR 8164 (1983) Folhas e Chapas de Aço Baixo Carbono—Determinação da Anisotropia Plástica e do Expoente de Encruamento, Brazil
13. Keeler SP (1965) Determination of forming limits in automotive stampings. Sheet Met Ind 42: 683–691

14. Narayanasamy R, Sathiya CS (2006) Some aspects on fracture limit diagram developed for different steel sheets. Mater Sci Eng, A 417:197–224
15. Sahu RK, Majumdar S, Prasad BN (2011) Forming limit diagram of high strength steel sheet (DP-590). MIT Int J Mech Eng 1–2:114–118
16. Nakazima KJ, Kikuma T, Hasuka K (1968) Study on formability of steel sheets. Yawata Tech Rep 264:141
17. Bucher JH, Hamburg EG (1977) SAE Trans 86.730, Sect. 1
18. DeArdo AJ, Garcia CI, Cho K, Hua M (2008) New method of characterizing and quantifying complex microstructures in steels. In: New developments on metallurgy and applications of high strength steels. Ternium, Tenaris and Asociacion Argentina de Materiales, Buenos Aires, Argentina, 22–26 May, pp 181–192
19. Uthaisangsuk V, Prahl U, Bleck W (2011) Modelling of damage and failure in multiphase high strength DP and TRIP steels. Eng Fract Mech 78:469–486
20. Ramazani A, Abbasi M, Prahl U, Bleck W (2012) Failure analysis of DP600 steel during the cross-die test. Comput Mater Sci 64:101–105
21. Lian J, Liu P, Münstermann S (2013) Modelling of damage and failure of dual phase steel in Nakajima test. Key Eng Mater 525–526:69–72